

SPIN-1/2 ASYMMETRIC DIAMOND ISING–HEISENBERG CHAIN

B.M. LISNII

PACS 75.10.Pq, 75.40.Cx,
75.10.Jm
©2011

Institute for Condensed Matter Physics, Nat. Acad. of Sci. of Ukraine
(1, Svetsits'kyi Str., Lviv 79011, Ukraine; e-mail: *lisnyj@icmp.lviv.ua*)

The ground state and the thermodynamics of a spin-1/2 asymmetric diamond Ising–Heisenberg chain are considered. For the XYZ anisotropic Heisenberg interaction, the exact calculations of the free energy, entropy, heat capacity, magnetization, and magnetic susceptibility are performed using the method of decoration-iteration transformation. In the case of antiferromagnetic interactions (Ising and XXZ anisotropic Heisenberg ones), the ground state, magnetization process, temperature dependence of the magnetization, magnetic susceptibility, and heat capacity are investigated. The influence of geometric frustration and quantum fluctuations on these characteristics is studied.

We consider a spin-1/2 asymmetric diamond Ising–Heisenberg chain with the XYZ anisotropic Heisenberg interaction between decoration spins. It has the same diamond structure as that considered in [9] and the same asymmetry of the Ising interaction on bonds along the diamond sides as in [14]. The decoration-iteration transformation [1, 2] is used to exactly calculate the thermodynamic characteristics of this chain. For the antiferromagnetic Ising interaction and the antiferromagnetic XXZ Heisenberg interaction, at which the system is geometrically frustrated, we consider the ground state, magnetization process, temperature dependence of the magnetization, magnetic susceptibility, and heat capacity. The effect of the Ising and Heisenberg interactions on these characteristics is studied.

1. Introduction

One of the interesting objects of statistical physics is exactly solvable decorated chains, whose structure is formed by the decoration of a primitive cell of a spin-1/2 Ising chain. The exact solution of these decorated chains is obtained using the method of decoration-iteration transformation [1, 2]. They particularly include the following one-dimensional models: spin-(1/2, $S > 1/2$) [3], ferromagnetic-ferromagnetic-antiferromagnetic [4], and diamond [5] Ising chains, simple [6–8], diamond [9, 10], tetrahedral [11], and sawtooth [12] Ising–Heisenberg chains, Ising–Heisenberg chain with triangular Heisenberg plaquettes [13], and asymmetric diamond Ising–Hubbard chain [14, 15]. Decorated chains are convenient objects for studying the appearance of intermediate plateaus on the magnetization curve and additional maxima on the temperature dependence of the heat capacity, as well as the mutual influence of the geometrical frustration and quantum fluctuations. All these phenomena take place in real systems [7, 16, 17].

2. Exact Solution of the Model

Consider a spin-1/2 asymmetric diamond Ising–Heisenberg chain in the magnetic field. A primitive cell of this chain is determined by nodes k and $k+1$ (Fig. 1). They are occupied by the so-called Ising spins ($\hat{\mu}_k^z$) coupled with neighbors by the Ising interaction. Two interstitial positions ($k, 1$) and ($k, 2$) in the primitive cell (Fig. 1) are occupied by the so-called Heisenberg spins ($\hat{S}_{k,1}$ and $\hat{S}_{k,2}$) with the Heisenberg interaction between them. We write the Hamiltonian of the chain $\hat{\mathcal{H}}$ as the sum of the cell Hamiltonians $\hat{\mathcal{H}}_k$:

$$\hat{\mathcal{H}} = \sum_{k=1}^N \hat{\mathcal{H}}_k,$$

$$\hat{\mathcal{H}}_k = J_1 \hat{S}_{k,1}^x \hat{S}_{k,2}^x + J_2 \hat{S}_{k,1}^y \hat{S}_{k,2}^y + J_3 \hat{S}_{k,1}^z \hat{S}_{k,2}^z +$$

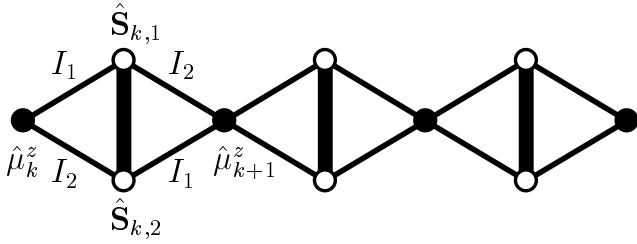


Fig. 1. Fragment of an asymmetric diamond Ising–Heisenberg chain. Spins $\hat{\mu}_k^z, \hat{\mu}_{k+1}^z$ at nodes and spins $\hat{\mathbf{S}}_{k,1}, \hat{\mathbf{S}}_{k,2}$ at interstitial positions of the k -th primitive cell are marked. The Ising interaction parameters on bonds along the diamond sides (I_1 and I_2) are different for samples with different orientations

$$\begin{aligned}
 & + \hat{\mu}_k^z (I_1 \hat{S}_{k,1}^z + I_2 \hat{S}_{k,2}^z) + \hat{\mu}_{k+1}^z (I_2 \hat{S}_{k,1}^z + I_1 \hat{S}_{k,2}^z) - \\
 & - \frac{h_I}{2} (\hat{\mu}_k^z + \hat{\mu}_{k+1}^z) - h_H (\hat{S}_{k,1}^z + \hat{S}_{k,2}^z), \quad (1)
 \end{aligned}$$

where N is the number of primitive cells; $\hat{\mu}_k^z$ and $\hat{S}_{k,i}^\alpha$ ($\alpha = x, y, z; i = 1, 2$) are the components of spin-1/2 operators; J_1, J_2 , and J_3 are the parameters of the Heisenberg interaction; I_1, I_2 are the parameters of the Ising interaction on the bonds along the diamond sides (Fig. 1); h_I and h_H are the magnetic fields acting on the Ising and Heisenberg spins, respectively. It is worth noting that Hamiltonian (1) also corresponds to a simple Ising–Heisenberg chain, in which the Ising spin interacts with the first (I_1) and second (I_2) neighbors. In the particular cases $I_1 = I_2$ and $I_2 = 0$ (or $I_1 = 0$), Hamiltonian (1) corresponds to the above-considered Ising–Heisenberg chains: diamond [9] and simple [6, 8] ones.

Let us find the statistical sum of the system $\mathcal{Z} = \text{Tr} e^{-\beta \hat{\mathcal{H}}}$, where $\beta = 1/k_B T$, k_B is the Boltzmann constant, and T is the absolute temperature. With regard for the commutativity of the Hamiltonians $\hat{\mathcal{H}}_k$, the statistical sum \mathcal{Z} is partially factorized:

$$\mathcal{Z} = \text{Tr}_{\{\hat{\mu}^z\}} \prod_{k=1}^N \text{Tr}_{\hat{\mathbf{S}}_{k,1}, \hat{\mathbf{S}}_{k,2}} \exp(-\beta \hat{\mathcal{H}}_k), \quad (2)$$

where $\text{Tr}_{\{\hat{\mu}^z\}}$ means the trace over the states of all Ising spins and $\text{Tr}_{\hat{\mathbf{S}}_{k,1}, \hat{\mathbf{S}}_{k,2}}$ is the trace over the states of two Heisenberg spins from the k -th cell. Now, we calculate the factor

$$\mathcal{Z}_k(\hat{\mu}_k^z, \hat{\mu}_{k+1}^z) = \text{Tr}_{\hat{\mathbf{S}}_{k,1}, \hat{\mathbf{S}}_{k,2}} \exp(-\beta \hat{\mathcal{H}}_k).$$

For this purpose, we should pass to the matrix representation of the Hamiltonian $\hat{\mathcal{H}}_k$ in the basis constructed by the eigenstates of the operator $\hat{S}_{k,1}^z \hat{S}_{k,2}^z$:

$$|\uparrow(\downarrow), \uparrow(\downarrow)\rangle_{k,1;k,2} = |\uparrow(\downarrow)\rangle_{k,1} |\uparrow(\downarrow)\rangle_{k,2},$$

where $|\uparrow\rangle_{k,i}$ and $|\downarrow\rangle_{k,i}$ denote the eigenstates of $\hat{S}_{k,i}^z$. The eigenvalues of the matrix $\hat{\mathcal{H}}_k$ have the form

$$\begin{aligned}
 \mathcal{E}_{1,2}(\hat{\mu}_k^z, \hat{\mu}_{k+1}^z) &= \frac{J_3}{4} - \frac{h_I}{2} (\hat{\mu}_k^z + \hat{\mu}_{k+1}^z) \pm \\
 & \pm \sqrt{\frac{(J_1 - J_2)^2}{16} + \left(\frac{I_1 + I_2}{2} (\hat{\mu}_k^z + \hat{\mu}_{k+1}^z) - h_H \right)^2},
 \end{aligned}$$

$$\begin{aligned}
 \mathcal{E}_{3,4}(\hat{\mu}_k^z, \hat{\mu}_{k+1}^z) &= -\frac{J_3}{4} - \frac{h_I}{2} (\hat{\mu}_k^z + \hat{\mu}_{k+1}^z) \pm \\
 & \pm \sqrt{\frac{(J_1 + J_2)^2}{16} + \frac{(I_1 - I_2)^2}{4} (\hat{\mu}_k^z - \hat{\mu}_{k+1}^z)^2}. \quad (3)
 \end{aligned}$$

Having obtained $\mathcal{Z}_k(\hat{\mu}_k^z, \hat{\mu}_{k+1}^z) = \sum_{i=1}^4 e^{-\beta \mathcal{E}_i(\hat{\mu}_k^z, \hat{\mu}_{k+1}^z)}$, we perform the decoration-iteration transformation [1, 2]:

$$\mathcal{Z}_k(\hat{\mu}_k^z, \hat{\mu}_{k+1}^z) = A \exp(\beta R \hat{\mu}_k^z \hat{\mu}_{k+1}^z + \beta h_0 (\hat{\mu}_k^z + \hat{\mu}_{k+1}^z)/2),$$

where A, R , and h_0 are the transformation parameters determined by the relations

$$A = (\mathcal{Z}_k(+, +) \mathcal{Z}_k(-, -) \mathcal{Z}_k^2(+, -))^{1/4},$$

$$\beta R = \ln \frac{\mathcal{Z}_k(+, +) \mathcal{Z}_k(-, -)}{\mathcal{Z}_k^2(+, -)}, \quad \beta h_0 = \ln \frac{\mathcal{Z}_k(+, +)}{\mathcal{Z}_k(-, -)},$$

in which the argument “ \pm ” means $\pm 1/2$. With the use of this transformation, the calculation of the statistical sum (2) of the Ising–Heisenberg chain is reduced to that of the statistical sum of the spin-1/2 Ising chain with interaction R and field h_0 . Applying the known result [18] to the latter, we obtain the statistical sum (2) in the form

$$\mathcal{Z} = A^N (\lambda_1^N + \lambda_2^N),$$

where

$$\lambda_{1,2} = e^{\beta R/4} \left(\text{ch}(\beta h_0/2) \pm \sqrt{\text{sh}^2(\beta h_0/2) + e^{-\beta R}} \right).$$

After that, the free energy of the cell in the thermodynamic limit takes the form

$$f = -\frac{1}{\beta} (\ln A + \ln \lambda_1),$$

which can be used for the calculation of the entropy s and the heat capacity c :

$$s = k_B \beta^2 \frac{\partial f}{\partial \beta}, \quad c = -\beta \frac{\partial s}{\partial \beta}.$$

The magnetization of the Ising spins $m_I = \langle \hat{\mu}_k^z + \hat{\mu}_{k+1}^z \rangle / 2$ and their correlation function $q_{II}(n) = \langle \hat{\mu}_k^z \hat{\mu}_{k+n}^z \rangle$ are the same as for the spin-1/2 Ising chain with interaction R and field h_0 [6, 8, 9]. That is why we can use the known results [18] for them. The magnetization of the Heisenberg spins $m_H = \langle \hat{S}_{k,1}^z + \hat{S}_{k,2}^z \rangle / 2$ can be obtained by the differentiation of the statistical sum (2) after applying the decoration-iteration transformation [8]:

$$m_H = \frac{1}{2\beta} \left(\frac{1}{A} \frac{\partial A}{\partial h_H} + q_{II}(1) \frac{\partial(\beta R)}{\partial h_H} + m_I \frac{\partial(\beta h_0)}{\partial h_H} \right).$$

From m_I and m_H , the summary magnetization can be determined as follows:

$$m = (m_I + 2m_H) / 3.$$

Now, let us calculate the susceptibility to the action of the magnetic field $h = h_I = h_H / r_g$, where r_g is the ratio of the g -factor of a Heisenberg spin to the g -factor of an Ising one:

$$\chi = \frac{\partial m}{\partial h} = \frac{1}{3} \left(\frac{\partial m_I}{\partial h_I} + \frac{\partial m_I}{\partial h_H} r_g \right) + \frac{2}{3} \left(\frac{\partial m_H}{\partial h_I} + \frac{\partial m_H}{\partial h_H} r_g \right).$$

In the particular cases $I_1 = I_2$ and $I_2 = 0$ (or $I_1 = 0$), the obtained results agree with the available data for diamond [9] and simple [6, 8] Ising-Heisenberg chains, respectively.

3. Numerical Results and Discussion

Consider the properties of a system with the antiferromagnetic Ising interaction ($I_1, I_2 > 0$) and the antiferromagnetic XXZ Heisenberg interaction: $J_1 = J_2 = J\Delta$, $J_3 = J$, where Δ is the interaction anisotropy parameter, $J > 0$. In this case, the system is geometrically frustrated. The magnetic fields h_I and h_H are supposed to be equal: $h = h_I = h_H$, i.e. $r_g = 1$. Without loss of generality, we assume that $I_1 \geq I_2$ and introduce the difference of the Ising interaction parameters $\Delta I = I_1 - I_2$ [14]. Passing to the dimensionless parameters, we have

$$\tilde{J} = \frac{J}{I_1}, \quad \Delta \tilde{I} = \frac{\Delta I}{I_1}, \quad \tilde{h} = \frac{h}{I_1}.$$

The parameter $\Delta \tilde{I}$ has a physical sense on the interval $[0, 1]$ and characterizes the degree of asymmetry of the Ising interaction at the bonds along the diamond sides.

First, we consider the properties of the ground state of the system. It corresponds to the lowest energy $\tilde{\mathcal{E}}_i = \mathcal{E}_i / I_1$ of spectrum (3) for the possible configurations $\hat{\mu}_k^z$ and $\hat{\mu}_{k+1}^z$. Depending on the parameters \tilde{J} , Δ , $\Delta \tilde{I}$, and \tilde{h} , the system can have four ground states: saturated paramagnetic state (SPA), ferrimagnetic state (FRI), unsaturated paramagnetic state (UPA), and nodal anti-ferromagnetic state (NAF). The energies of these states for the initial cell are as follows:

$$\tilde{\mathcal{E}}_{\text{SPA}} = \frac{\tilde{J}}{4} + 1 - \frac{\Delta \tilde{I}}{2} - \frac{3\tilde{h}}{2},$$

$$\tilde{\mathcal{E}}_{\text{FRI}} = \frac{\tilde{J}}{4} - 1 + \frac{\Delta \tilde{I}}{2} - \frac{\tilde{h}}{2},$$

$$\tilde{\mathcal{E}}_{\text{UPA}} = -\frac{\tilde{J}}{4} - \frac{\tilde{J}\Delta}{2} - \frac{\tilde{h}}{2},$$

$$\tilde{\mathcal{E}}_{\text{NAF}} = -\frac{\tilde{J}}{4} - \frac{1}{2} \sqrt{\tilde{J}^2 \Delta^2 + \Delta \tilde{I}^2}.$$

The wave functions of these states have the form

$$|\text{SPA}\rangle = \prod_{k=1}^N |+\rangle_k | \uparrow, \uparrow \rangle_{k,1;k,2},$$

$$|\text{FRI}\rangle = \prod_{k=1}^N |-\rangle_k | \uparrow, \uparrow \rangle_{k,1;k,2},$$

$$|\text{UPA}\rangle = \begin{cases} \prod_{k=1}^N |+\rangle_k \left[\frac{1}{\sqrt{2}} (| \uparrow, \downarrow \rangle - | \downarrow, \uparrow \rangle) \right]_{k,1;k,2} & \text{for } \Delta \neq 0, \\ \prod_{k=1}^N |+\rangle_k \left| \begin{smallmatrix} \uparrow, \downarrow \\ \downarrow, \uparrow \end{smallmatrix} \right\rangle_{k,1;k,2} & \text{for } \Delta = 0, \end{cases}$$

$$|\text{NAF}\rangle = \prod_{k=1}^N \left| (- \right)^{n=\{ \begin{smallmatrix} k \\ k+1 \end{smallmatrix} \}} \rangle_k \times \\ \times \left[A^{(-)n} | \uparrow, \downarrow \rangle - A^{(-)n+1} | \downarrow, \uparrow \rangle \right]_{k,1;k,2},$$

where the vectors $|\pm\rangle_k$ describe the state of the spins $\hat{\mu}_k^z$: $|+\rangle_k = | \uparrow \rangle_k$, $|-\rangle_k = | \downarrow \rangle_k$. The wave functions of the doubly degenerated NAF state are written down with the help of the expression $(-)^n \in \{-, +\}$ that means

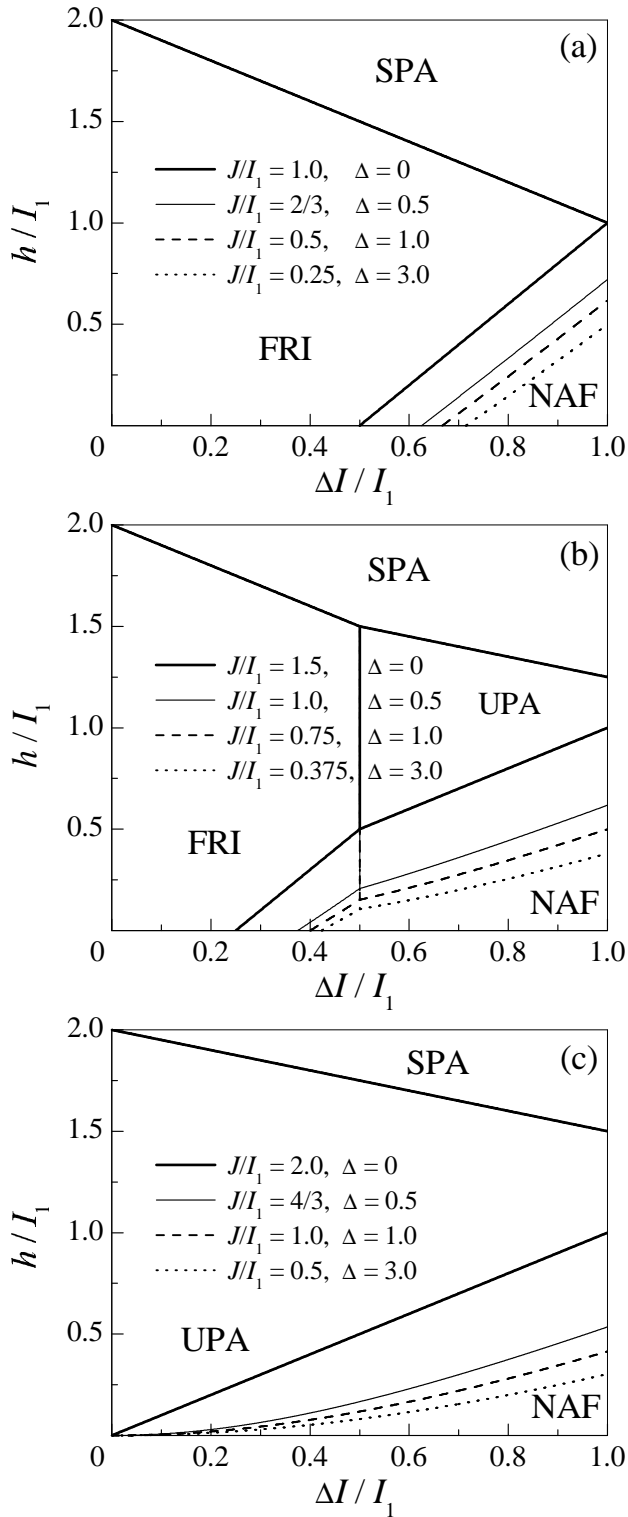


Fig. 2. Ground-state phase diagram $(\Delta\tilde{I}, \tilde{h})$ as a function of \tilde{J} and Δ . Three characteristic topologies are shown: (a), (b), and (c) with transition lines for several sets of values of \tilde{J} and Δ

the sign of the number $(-1)^n$. The coefficients A^\pm are as follows:

$$A^\pm = \frac{1}{\sqrt{2}} \sqrt{1 \mp \frac{\Delta\tilde{I}}{\sqrt{\tilde{J}^2\Delta^2 + \Delta\tilde{I}^2}}}$$

In the UPA state at $\Delta = 0$, the pair of spins $\hat{S}_{k,1}$ and $\hat{S}_{k,2}$ occupies one of the two equiprobable states $|\uparrow, \downarrow\rangle_{k,1;k,2}$ and $|\downarrow, \uparrow\rangle_{k,1;k,2}$. That is why this state is macroscopically degenerated and has the residual entropy $s_{\text{res}} = k_B \ln 2$.

The ground-state phase diagram $(\Delta\tilde{I}, \tilde{h})$ can have topology of three types depending on $\tilde{J}(1 + \Delta)$ (Fig. 2). The phase diagram with topology of type 1 (Fig. 2, a) includes the FRI, NAF, and SPA states. It is realized at $\tilde{J}(1 + \Delta) \leq 1$. In the zero field, the FRI and NAF states are separated by the critical point

$$\Delta\tilde{I}_{\text{F.N}} = \frac{2 - \tilde{J}}{2} - \frac{\tilde{J}^2\Delta^2}{2(2 - \tilde{J})}$$

It is worth noting that, in the FRI state, there arises the geometrical frustration effect on the Heisenberg bond: the pair of Heisenberg spins occupies the ferromagnetic state $|\uparrow, \uparrow\rangle_{k,1;k,2}$ that does not correspond to the minimum of the energy $J\hat{S}_{k,1}^z\hat{S}_{k,2}^z$. In the NAF state, one observes the effect of quantum fluctuations on this bond: the pair of Heisenberg spins occupies the mixed states $[A^\mp|\uparrow, \downarrow\rangle - A^\pm|\downarrow, \uparrow\rangle]_{k,1;k,2}$ with the minimum energy $J\hat{S}_{k,1}^z\hat{S}_{k,2}^z$. The phase diagram with topology of type 2 (Fig. 2, b) includes all the ground states and is realized at $1 < \tilde{J}(1 + \Delta) < 2$. The FRI and UPA states are separated by the line $\Delta\tilde{I} = \Delta\tilde{I}_{\text{F|U}}$, where $\Delta\tilde{I}_{\text{F|U}} = 2 - \tilde{J}(1 + \Delta)$. The phase diagram with topology of type 3 (Fig. 2, c) includes the NAF, UPA, and SPA states. It is realized at $2 \leq \tilde{J}(1 + \Delta)$. The line of transition between the NAF and UPA states starts at the point $(0, 0)$. In Fig. 2, one can see that the interval $(0, \Delta\tilde{I}_{\text{F.N}})$, in which there arises the geometrical frustration effect on the Heisenberg bond, decreases to zero due to the intensification of quantum fluctuations.

The SPA and FRI states are identical, whereas the UPA (except for the case of $\Delta = 0$) and NAF states are isomorphous to the corresponding states of an asymmetric diamond Ising–Hubbard chain [14, 15]. The typical topologies of the ground-state phase diagram $(\Delta\tilde{I}, \tilde{h})$ are also the same as those for this chain [14, 15]. That is why the specific features of the ground state at the critical points of the phase diagrams $(\Delta\tilde{I}, \tilde{h})$ described in [15] are also observed at the corresponding points in Fig. 2 at $\Delta \neq 0$. At $\Delta = 0$, the ground-state characteristics at

the critical points, where the UPA state is realized, can have values other than those at $\Delta \neq 0$. In particular, at the critical point $(0, 0)$ in Fig. 2, *c*, the residual entropy at $\Delta = 0$ is larger than that at $\Delta \neq 0$, namely $s_{\text{res}} = k_B \ln 5$ for $\tilde{J} = 2$ and $s_{\text{res}} = k_B \ln 4$ for $\tilde{J} > 2$, where the ground state is frustrated [15]. In addition, the ground state of our system has interesting peculiarities at $\tilde{J} = 1$ and $\Delta = 0$ at the critical point $(1, 1)$ in Fig. 2, *a*. It is the only point of coexistence of all the ground states (SPA, FRI, NAF, and UPA). In addition, it is the point, at which the nodal antiferromagnetic state NAF₊ is realized with the energy $\tilde{\mathcal{E}}_{\text{NAF}_+} = \tilde{J}/4 - \tilde{h}$ and the wave function

$$|\text{NAF}_+\rangle = \prod_{k=1}^N \left| (-)^{n=\left\{ \begin{smallmatrix} k \\ k+1 \end{smallmatrix} \right\}} \right\rangle_k \left| \uparrow, \uparrow \right\rangle_{k,1;k,2}.$$

The Ising subsystem has the characteristics

$$\beta R = \ln \frac{3}{4}, \quad \beta h_0 = \ln 3, \quad m_{\text{I}} = \frac{m_{\text{s}}}{\sqrt{5}}, \quad q_{\text{II}}(n) = \frac{1 + 4(4\sqrt{5} - 9)^n}{20},$$

where $m_{\text{s}} = 1/2$ is the saturation magnetization. In this ground state, $R = h_0 = 0$, but Ising spins are not effectively free, because the temperature dependence of R and h_0 has a linear component [15]. This ground state has $s_{\text{res}} = k_B \ln(2 + \sqrt{5})$.

The ground-state phase diagrams $(\Delta\tilde{I}, \tilde{h})$ in Fig. 2 demonstrate the following regularities. The diamond Ising–Heisenberg chain can have the NAF ground state if $\Delta\tilde{I} \neq 0$ in the chain. The simple diamond Ising–Heisenberg chain can have the FRI ground state in the zero field, if the interaction of an Ising spin with second neighbors is strong enough ($\Delta\tilde{I} < 1$).

Now, we consider the influence of the Heisenberg interaction on the ground-state phase diagram $(\Delta\tilde{I}, \tilde{h})$. In the case if the energy $\tilde{\mathcal{E}}_{\text{UPA}}$ remains constant with respect to the energy $\tilde{\mathcal{E}}_{\text{FRI}}$ (which means that it also remains constant with respect to $\tilde{\mathcal{E}}_{\text{SPA}}$), a change of \tilde{J} and Δ gives rise to a much simpler reconstruction of the phase diagram $(\Delta\tilde{I}, \tilde{h})$ than their independent variation. Let us determine the constant of this condition at the point $(\tilde{J} = \tilde{J}^*, \Delta = 0)$, where the Heisenberg interaction is converted to the Ising one \tilde{J}^* . As a result, we obtain the interrelation of \tilde{J} and Δ as follows:

$$\tilde{J} + \tilde{J}\Delta = \tilde{J}^*. \quad (4)$$

According to the above-described dependence of the topology of the phase diagram $(\Delta\tilde{I}, \tilde{h})$ on the Heisenberg interaction, the topologically equivalent phase diagrams $(\Delta\tilde{I}, \tilde{h})$ are obtained in mode (4). The change of the phase diagram $(\Delta\tilde{I}, \tilde{h})$ in mode (4) is shown in Fig. 2,

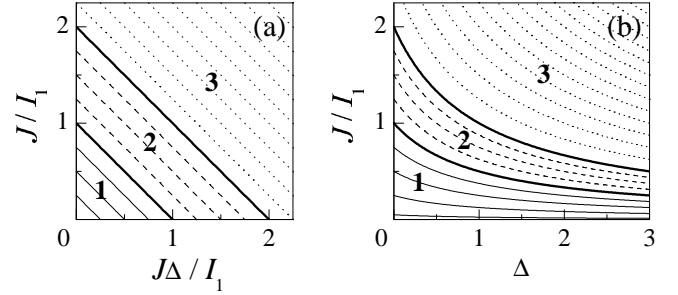


Fig. 3. Topological diagrams $(\tilde{J}\Delta, \tilde{J})$ (a) and (Δ, \tilde{J}) (b) of the ground-state phase diagram $(\Delta\tilde{I}, \tilde{h})$ covered by “equitopological” lines (4). Thick lines mark the boundary between the regions of three typical topologies specified by the corresponding numbers

where the sets of values \tilde{J} and Δ for each case (*a*, *b*, or *c*) correspond to a certain \tilde{J}^* . One can see that this change consists in a shift of the lines of the NAF \leftrightarrow FRI and NAF \leftrightarrow UPA transitions. Based on the above consideration, a diagram reflecting the influence of the Heisenberg interaction on the topology of the phase diagram $(\Delta\tilde{I}, \tilde{h})$ can be constructed. Such a topological diagram is presented in Fig. 3 in two planes: $(\tilde{J}\Delta, \tilde{J})$ and (Δ, \tilde{J}) . The topological diagram $(\tilde{J}\Delta, \tilde{J})$ illustrates the fact that the topology of the phase diagram $(\Delta\tilde{I}, \tilde{h})$ depends on the *ZZ*- and *XY*-components of the Heisenberg interaction in the same way.

Let us consider the magnetization process and thermodynamic characteristics as functions of the temperature and their dependence on the Ising interaction asymmetry and Heisenberg interaction parameters in mode (4). For this purpose, we select sets of values of \tilde{J} and Δ , the ground-state phase diagram $(\Delta\tilde{I}, \tilde{h})$ for which is depicted in Fig. 2, *b*. The summary magnetization as a function of the field for different temperatures and as a function of the temperature for different fields is presented for two characteristic cases: the FRI ground state in the zero field (Fig. 4) and the NAF ground state in the zero field (Fig. 5). The field dependence of the summary magnetization at the zero temperature in Fig. 4, *a* has an intermediate plateau $m/m_{\text{s}} = 1/3$ corresponding to the FRI ground state, whereas in Fig. 5, *a*, there are two intermediate plateaus: $m/m_{\text{s}} = 0$ corresponding to the NAF ground state and $m/m_{\text{s}} = 1/3$ corresponding to the UPA ground state. The magnetization m/m_{s} in Fig. 4, *b* in the critical field of the FRI \leftrightarrow SPA transition tends to $2/3$ as the temperature approaches zero. In Fig. 5, *b*, the magnetization m/m_{s} in the lower and upper critical fields corresponding to the NAF \leftrightarrow UPA and UPA \leftrightarrow SPA transitions tends to $1/(3\sqrt{5})$ and $2/3$, respectively. The Heisenberg interaction significantly influences the field dependence of m at low temperatures

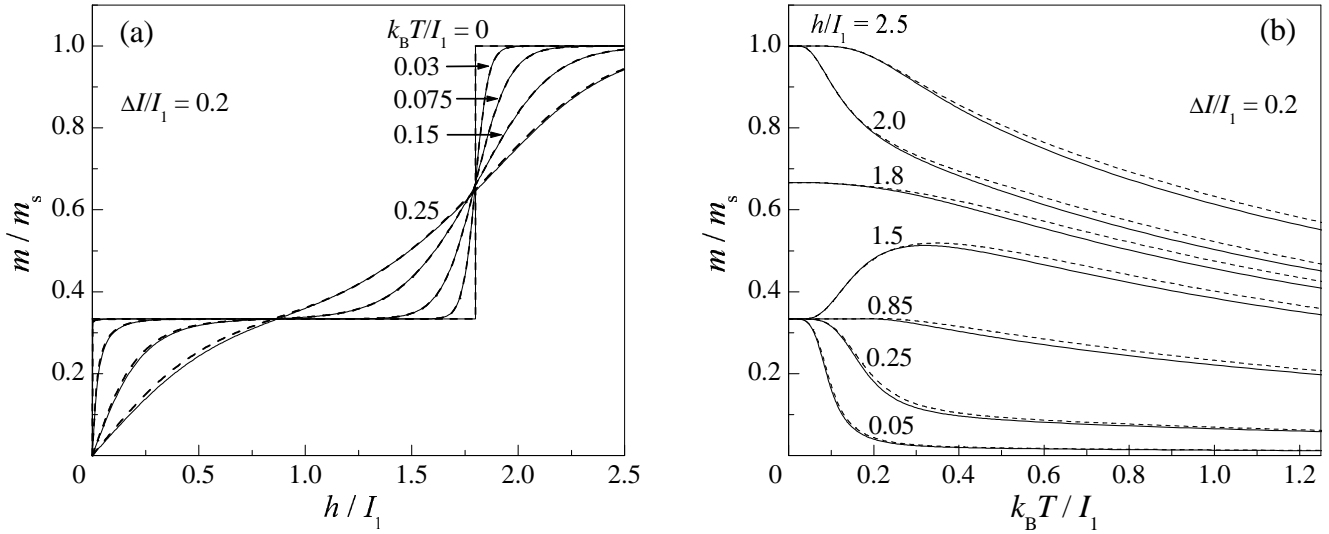


Fig. 4. Summary magnetization as a function of the field for different temperatures (a) and as a function of the temperature for different fields (b) in the case of the FRI ground state in the zero field. Solid lines mark the results obtained for $\tilde{J} = 1.0$ and $\Delta = 0.5$, dashed lines – those obtained for $\tilde{J} = 0.375$ and $\Delta = 3$

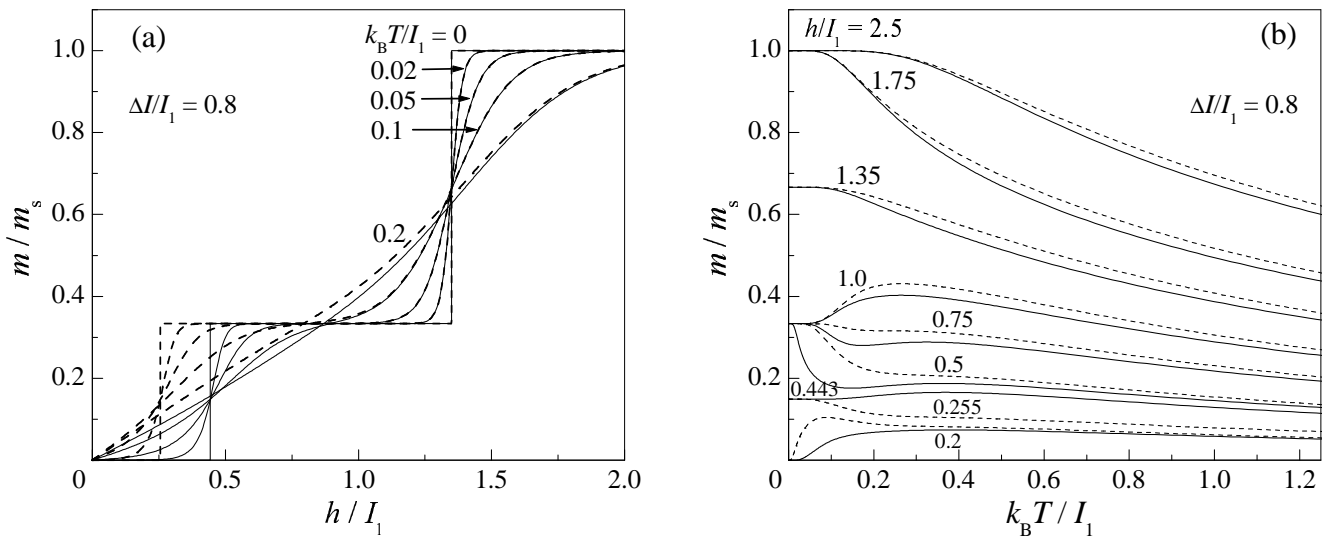


Fig. 5. Summary magnetization as a function of the field for different temperatures (a) and as a function of the temperature for different fields (b) in the case of the NAF ground state in the zero field. Solid lines mark the results obtained for $\tilde{J} = 1.0$ and $\Delta = 0.5$, dashed lines – those obtained for $\tilde{J} = 0.375$ and $\Delta = 3$

in the field range belonging to the region of the NAF ground state and a certain part of the neighboring region (Fig. 5,a). As a result, it also has some effect on the low-temperature dependence of m for fields belonging to this region (Fig. 5,b). Due to the intensification of quantum fluctuations, the temperature curve of m shifts upward in the region of medium and high temperatures (Fig. 4,b and Fig. 5,b). This increment of m is a result of the decrease of m_I due to a reduction of the effective

field h_0 , as well as the increase of m_H due to the relative growth of the energies $\hat{\mathcal{H}}_k$ (3) corresponding to states with zero magnetization of the Heisenberg spins.

The magnetic susceptibility multiplied by the temperature ($\chi k_B T$) as a function of the temperature in the zero field is presented in Fig. 6. With the FRI ground state in the zero field, this dependence looks like that for quantum ferrimagnetics [19], while, in the case of the NAF ground state in the zero field, it has an antiferromagnetic

character. As the temperature tends to zero, the quantity $\chi k_B T$ can either exponentially diverge (if $\Delta \tilde{I}$ corresponds to the FRI ground state), or exponentially tends to zero (if $\Delta \tilde{I}$ corresponds to the NAF ground state), or takes the value of $1/12$ (if $\Delta \tilde{I}$ appears exactly in the critical point $\Delta \tilde{I}_{F,N}$). The low-temperature dependence of $\chi k_B T$ strongly reacts to a variation of the quantum fluctuation intensity, if $\Delta \tilde{I}$ appears in some neighborhood of the critical point $\Delta \tilde{I}_{F,N}$ or above it (Fig. 6). The high-temperature dependence of $\chi k_B T$ shifts to a higher susceptibility with increase in the intensity of quantum fluctuations.

For a certain interval of $\Delta \tilde{I}$ widening with increase in the quantum fluctuation intensity, the temperature dependence of the heat capacity in the zero field has two maxima: principal and low-temperature ones (Fig. 7). At $\Delta = 0$, it particularly has two maxima for $\Delta \tilde{I} \in (0.16, 0.31)$, and one intense low-temperature maximum beyond this interval that considerably changes with the appearance of weak quantum fluctuations (Fig. 7). An increase of their intensity results in a considerable growth of the height of the principal maximum and a decrease of its temperature. With their further intensification, however, the height of the principal maximum decreases, while its temperature rises (Fig. 7). The growth of $\Delta \tilde{I}$ in the interval $(0, \Delta \tilde{I}_{F,N})$ results in a reduction of the height of the principal maximum and the rise of its temperature, whereas, in the interval $(\Delta \tilde{I}_{F,N}, 1)$, the situation is opposite. The low-temperature maximum is mainly caused by thermal excitations responsible for the transitions between the FRI, NAF, and UPA states. Its height and temperature considerably change due to the variation of the intensity of quantum fluctuations, if $\Delta \tilde{I}$ lies in a certain vicinity of the critical point $\Delta \tilde{I}_{F,N}$ or above it (Fig. 7). With increase in $\Delta \tilde{I}$, its temperature noticeably falls for $\Delta \tilde{I} < \Delta \tilde{I}_{F,N}$ and grows for $\Delta \tilde{I} > \Delta \tilde{I}_{F,N}$. If $\Delta \tilde{I}$ appears in a rather close vicinity of the critical point $\Delta \tilde{I}_{F,N}$, the thermal excitation corresponding to the energy of the FRI \leftrightarrow NAF transition gives rise to the formation of an additional low-temperature maximum close to the zero temperature. The formation and evolution of this maximum depending on $\Delta \tilde{I}$ takes place similarly to the heat capacity of an asymmetric diamond Ising–Hubbard chain [15].

4. Conclusions

The ground state and the thermodynamics of a spin-1/2 asymmetric diamond Ising–Heisenberg chain are investigated. Exact calculations of the free energy, entropy, heat capacity, magnetization of Ising and Heisen-

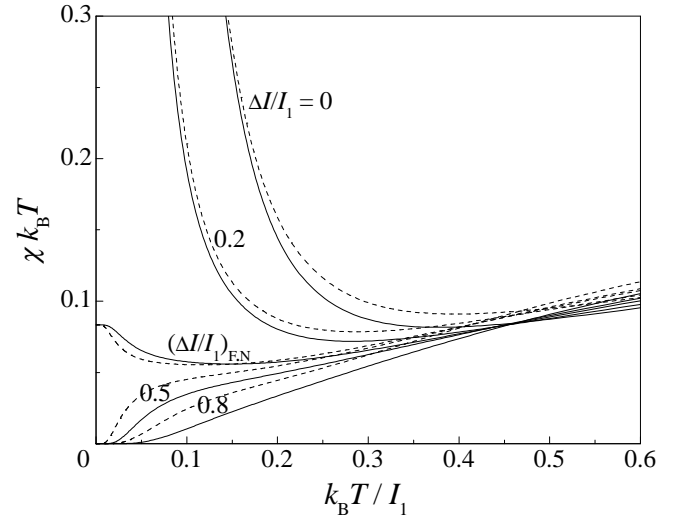


Fig. 6. Magnetic susceptibility multiplied by the temperature as a function of the temperature in the zero field. Solid lines mark the results obtained for $\tilde{J} = 1.0$ and $\Delta = 0.5$, dashed lines – those obtained for $\tilde{J} = 0.375$ and $\Delta = 3$

berg spins, and magnetic susceptibility are performed by the method of decoration-iteration transformation for the XYZ anisotropic Heisenberg interaction. In the case of the antiferromagnetic Ising interaction and antiferromagnetic XXZ Heisenberg interaction, with the system being geometrically frustrated, the ground state, field and temperature dependences of the magnetization, and temperature dependence of the magnetic susceptibility and of the heat capacity in zero field are investigated. The influence of the asymmetry parameter of the Ising interaction ($\Delta \tilde{I}$) and the Heisenberg interaction parameters (\tilde{J} and Δ) on these characteristics in the mode $\tilde{J} + \tilde{J}\Delta = \text{const}$ (4) is studied.

The geometrically frustrated system under study has four ground states: SPA, FRI, UPA, and NAF. Its ground state phase diagram $(\Delta \tilde{I}, \tilde{h})$ has three typical topologies, which is similar to the situation observed in the case of an asymmetric diamond Ising–Hubbard chain [14, 15]. A variation of the Heisenberg interaction parameters in mode (4) does not change the topology of the phase diagram $(\Delta \tilde{I}, \tilde{h})$; it only shifts the boundaries of the NAF ground state at the latter. The topology of the phase diagram $(\Delta \tilde{I}, \tilde{h})$ depending on the Heisenberg interaction is described by the topological diagrams $(\tilde{J}\Delta, \tilde{J})$ and (Δ, \tilde{J}) . It is shown that, at the zero temperature, rather strong quantum fluctuations remove the geometrical frustration effect on the Heisenberg bond.

The intensification of quantum fluctuations results in an increase of the summary magnetization and the mag-

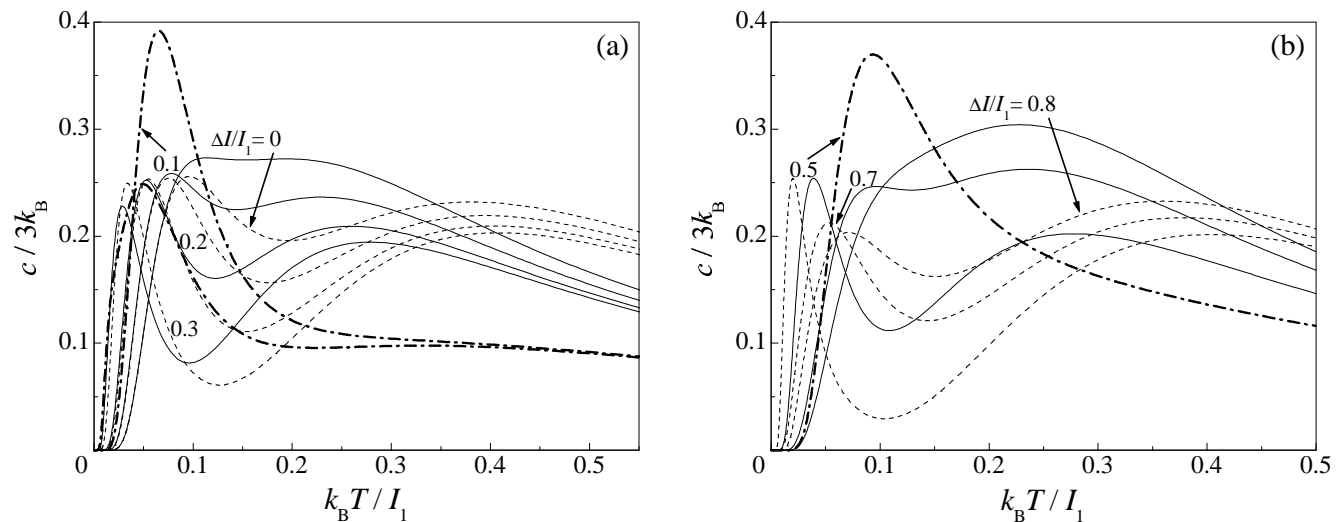


Fig. 7. Temperature dependence of the heat capacity in the zero field at $\Delta\tilde{I} < \Delta\tilde{I}_{F,N}$ (a) and $\Delta\tilde{I} > \Delta\tilde{I}_{F,N}$ (b). Dash-and-dot lines mark the results obtained for $\tilde{J} = 1.5$ and $\Delta = 0$, solid lines – for $\tilde{J} = 1.0$ and $\Delta = 0.5$, and dashed lines – for $\tilde{J} = 0.375$ and $\Delta = 3$

netization of Heisenberg spins and in a decrease of the magnetization of Ising spins in the region of medium and high temperatures. In this case, a growth of the magnetic susceptibility in the zero field is observed. The temperature dependence of the heat capacity in the zero field has a principal maximum and a low-temperature one for a certain interval of $\Delta\tilde{I}$ widening with increase in the quantum fluctuation intensity. The heights and the temperatures of these maxima can significantly change depending on the strength of quantum fluctuations and noticeably change depending on $\Delta\tilde{I}$. If $\Delta\tilde{I}$ lies in a rather close vicinity of the critical point $\Delta\tilde{I}_{F,N}$, the heat capacity has another low-temperature maximum caused by the transition between the FRI and NAF states.

The obtained results are also valid for a simple Ising–Heisenberg chain, in which an Ising spin interacts with the first and second neighbors. In the limiting cases $I_1 = I_2$ ($\Delta\tilde{I} = 0$) and $I_2 = 0$ ($\Delta\tilde{I} = 1$), these results correspond to the earlier considered diamond [9] and simple [6, 8] Ising–Heisenberg chains.

The author is grateful to Prof. O.V. Derzhko and Dr. T.M. Verkholyak for the discussion and useful remarks.

1. I. Syozi, Prog. Theor. Phys. **6**, 341 (1951).
2. M. Fisher, Phys. Rev. **113**, 969 (1959).
3. T. Kaneyoshi, Prog. Theor. Phys. **97**, 407 (1997).
4. V.R. Ohanyan and N.S. Ananikian, Phys. Lett. A **307**, 76 (2003).

5. J.S. Valverde, O. Rojas, and S.M. de Souza, Physica A **387**, 1947 (2008).
6. J. Strečka and M. Jaščur, J. Phys.: Cond. Matter **15**, 4519 (2003).
7. J. Strečka, M. Jaščur, M. Hagiwara, K. Minami, Y. Narumi, and K. Kindo, Phys. Rev. B **72**, 024459 (2005).
8. B.M. Lisnii, Ukr. Fiz. Zh. **53**, 712 (2008).
9. L. Čanová, J. Strečka, M. Jaščur, J. Phys.: Cond. Matter **18**, 4967 (2006).
10. L. Čanová, J. Strečka, T. Lučivjanský, Condens. Matter Phys. **12**, 353 (2009).
11. J.S. Valverde, O. Rojas, and S.M. de Souza, J. Phys.: Condens. Matter **20**, 345208 (2008).
12. V. Ohanyan, Condens. Matter Phys. **12**, 343 (2009).
13. D. Antonosyan, S. Bellucci, and V. Ohanyan, Phys. Rev. B **79**, 014432 (2009).
14. M.S.S. Pereira, F.A.B.F. de Moura, and M.L. Lyra, Phys. Rev. B **77**, 024402 (2008).
15. B.M. Lisnii, Fiz. Nizk. Temp. **37**, 380 (2011).
16. H. Kikuchi, Y. Fujii, M. Chiba, S. Mitsudo, T. Idehara, T. Tonegawa, K. Okamoto, T. Sakai, T. Kuwai, and H. Ohta, Phys. Rev. Lett. **94**, 227201 (2005).
17. H. Kikuchi, Y. Fujii, M. Chiba, S. Mitsudo, T. Idehara, T. Tonegawa, K. Okamoto, T. Sakai, T. Kuwai, and H. Ohta, Prog. Theor. Phys. Suppl. **159**, 1 (2005).
18. R.J. Baxter, *Exactly Solved Models in Statistical Mechanics* (Academic Press, London, 1982).
19. S. Yamamoto, Phys. Rev. B **59**, 1024 (1999).

Received 12.04.11.

Translated from Ukrainian by H.G. Kalyuzhna

СПІН-1/2 АСИМЕТРИЧНИЙ РОМБІЧНИЙ ЛАНЦЮЖОК
ІЗИНГА-ГАЙЗЕНБЕРГА*Б.М. Лісний*

Резюме

Розглянуто основний стан і термодинаміку спін-1/2 асиметричного ромбічного ланцюжка Ізинга-Гайзенберга. Для XYZ анізотропної взаємодії Гайзенберга методом декораційно-ітера-

ційного перетворення точно розраховано вільну енергію, ентропію, теплоємність, намагніченість і магнітну сприйнятливість. У випадку антиферромагнітних взаємодій – Ізинга і XXZ анізотропної Гайзенберга – досліджено основний стан, процес намагнічування, температурну залежність намагніченості, магнітної сприйнятливості і теплоємності. Вивчено вплив геометричної фрустрації та квантових флуктуацій на ці характеристики.